

Constraining Light Dependency in Modeled Emissions Through Comparison to Observed BVOC Concentrations in a Southeastern US Forest

Namrata Shanmukh Panji¹, Deborah F. McGlynn¹, Laura E. R. Barry², Todd M. Scanlon², Manuel T. Lerdau², Sally E. Pusede², and Gabriel Isaacman-VanWertz¹

¹Department of Civil and Environmental Engineering, Virginia Tech, Blacksburg, VA, 24061, USA

²Department of Environmental Sciences, University of Virginia, Charlottesville, VA 22904, USA

Correspondence: Namrata Shanmukh Panji (namratapanji@vt.edu) and Gabriel Isaacman-VanWertz (ivw@vt.edu)

Abstract. Climate change will bring about changes in meteorological and ecological factors that are currently used in global-scale models to calculate biogenic emissions. By comparing long-term datasets of biogenic compounds to modeled emissions, this work seeks to improve understanding of these models and their driving factors. We compare speciated BVOC measurements at the Virginia Forest Research Laboratory located in Fluvanna County, VA, USA for the 2020 year with emissions estimated by MEGANv3.2. The emissions were subjected to oxidation in a 0-D box-model (F0AM v4.3) to generate timeseries of modeled concentrations. We find that default light-dependent fractions (LDFs) in the emissions model do not accurately represent observed temporal variability of regional observations. Some monoterpenes with a default light dependence are better represented using light-independent emissions throughout the year ($LDF_{\alpha\text{-pinene}}=0$, as opposed to 0.6), while others are best represented using a seasonally or temporally dependent light dependence. For example, limonene has the highest correlation between modeled and measured concentrations using a $LDF=0$ for January through April and roughly 0.74-0.97 in the summer months, in contrast to the default value of 0.4. The monoterpenes β -thujene, sabinene, and γ -terpinene similarly have an LDF that varies throughout the year, with light-dependent behavior in summer, while camphene and α -fenchene follow light-independent behavior throughout the year. Simulations of most compounds are consistently underpredicted in the winter months compared to observed concentrations. In contrast, day-to-day variability in the concentrations during summer months are relatively well captured using the coupled emissions-chemistry model constrained by regional concentrations of NO_x and O_3 .

1 Introduction

Reactive organic gases are released into the atmosphere on the scale of $\sim 935 \text{ Tg C}$ per year (Safieddine et al., 2017) and are a critical area of research due to their role in forming ozone and particulate matter, which in-turn have detrimental effects on human health, climate change, and air quality (Ebi and McGregor, 2008). Roughly 90% of non-methane organic carbon is emitted as biogenic volatile organic compounds (BVOCs), from natural sources (Guenther et al., 1995) such as the regular metabolic processes of vegetation and microbial material (Goldstein and Galbally, 2007). Subsequent photochemistry of

these compounds results in the formation of secondary pollutants such as tropospheric ozone and secondary organic aerosols (SOA) (Atkinson, 2000; Atkinson and Arey, 2003; Guenther et al., 1995). Exposure to tropospheric ozone and SOA can cause 25 short-term effects like eye, nose, throat irritation, and respiratory symptoms. Prolonged exposure may lead to severe issues like increased cancer risk, and Central Nervous System (CNS), liver, and kidney damage, particularly in vulnerable populations (Kampa and Castanas, 2008). Apart from their effects on human health, they cause radiative forcing that impacts global temperatures (Myhre et al., 2014).

BVOC emissions are influenced by various environmental factors, including temperature, light, ozone levels, and other 30 meteorological conditions. Higher temperatures often lead to increased BVOC emissions due to enhanced metabolic activity in plants (Dindorf et al., 2006; Rasmussen and Went, 1965) and conversely, BVOC emissions can alleviate temperature stresses (Holopainen, 2004; Holopainen and Gershenson, 2010). Light availability plays a crucial role in the regulation of emissions, with higher radiation levels stimulating photosynthesis and subsequent BVOC production (Sanadze, 1969; Lerdau and Gray, 2003; Dindorf et al., 2006; Li and Sharkey, 2013). Ozone levels can also influence BVOC emissions, with elevated ozone 35 concentrations exacerbating or inhibiting emission rates depending on duration of exposure (Calfapietra et al., 2013; Lu et al., 2019). However, most studies investigate these effects at the leaf-level or tree-level (Yu and Blande, 2021; Chen et al., 2020; Huang et al., 2018; Kivimäenpää et al., 2016; Helmig et al., 2007) and extrapolation to canopy- or ecosystem-scale impacts can be complex. Furthermore, it can be difficult to decouple multiple competing or complementary effects, such as the chemical 40 destruction of emitted BVOCs by increased ozone masking potential increased emissions, or changes in stomatal uptake under differing conditions (Fiscus et al., 2005; Herbinger et al., 2007) impacting both BVOC and ozone emission and uptake (Sadiq et al., 2017; Zheng et al., 2015).

In addition to the sensitivity of BVOC emissions to meteorological conditions, they also exhibit plant species-specificity and physiology-specificity (Llusia et al., 2008). Hence, BVOCs are emitted at varying rates and composition due to the different plant species available in a forest ecosystem, and factors such as their leaf age, plant health, and seasonality. Previously, studies have investigated observed temporal BVOC trends on an ecosystem level (Lindwall et al., 2015; Debevec and Sauvage, 2023) and others have modeled global BVOC emissions (Guenther et al., 2006). Global and/or regional BVOC emissions can be estimated using EPA BEIS (Environmental Protection Agency Biogenic Emissions Inventory System available at <https://www.epa.gov/air-emissions-modeling/biogenic-emission-inventory-system-beis>) and the Model of Emissions of Gases and Aerosols from Nature (MEGANv3.2 available at <https://bai.ess.uci.edu/megan/data-and-code/megan32>). In previous comparisons with short-term observations, MEGAN has been shown to be in good agreement for some compounds and some ecosystems, but have discrepancies in other cases (Sindelarova et al., 2014). The model has been shown to overpredict night-time monoterpene emissions due to combining both light- and temperature-dependent effects to calculate monoterpene emissions (Emmerson et al., 2018; Sindelarova et al., 2014). However, the design of MEGAN to couple with different chemical transport mechanisms has allowed regional and global studies of BVOC concentrations (Situ et al., 2013; Emmerson et al., 55 2018), secondary organic aerosol formation (Yang et al., 2011), and ozone production (Liu et al., 2018). Seasonal variations in BVOC emissions are sensitive to temperature-dependent factors and leaf area index (Zhang et al., 2021).

Many of the parameters used by default in MEGAN have been estimated as global averages, but variation is possible in these parameters to better reflect local or regional conditions. Of particular interest to this work is the light-dependence of monoterpenes. Emmerson et al. (2018) studied the effect of light-dependence of monoterpene emissions in MEGAN in southeastern Australia where they concluded that disabling the monoterpene light-dependence improved the otherwise underpredicted local monoterpene estimations. Analysis of long-term speciated BVOC concentrations at our research site in a southeastern US forest has shown that some monoterpenes exhibit light-independent behavior, despite light-dependent defaults in the model, while others have seasonally-dependent light-dependence (McGlynn et al., 2023a), which is not a default capability of the model. In this study, we aim to enhance our understanding of BVOC emissions by probing the species-specific temporal variations of light-dependent fractions to better represent the observations at a regional-scale southeastern US forest.

2 Methods

2.1 Ground-based measurements

BVOC concentrations. Mixing ratios of BVOCs were measured at the Virginia Forest Research Laboratory (VFRL) in Palmyra, Virginia (37.9229°N, 78.2739°W) using an automated gas chromatograph with flame ionization detector (GC-FID) system (McGlynn et al., 2023b). The sample is collected 20m above ground, approximately in the middle of the tree canopy, and passed through a sodium thiosulfate-infused quartz filter (Pollmann et al., 2005) to scrub for ozone. It is then collected onto a multi-bed adsorbent trap which is thermally desorbed once every hour for analysis by the GC-FID (McGlynn et al., 2021). Further details about the instrumental setup, its calibration and operation are available in (McGlynn et al., 2021) and McGlynn et al. (2023b). Currently, 2 years of BVOC mixing ratios are available (McGlynn, 2022) but in this study, we focus on measurements made between January 1, 2020 and December 31st, 2020.

Meteorological data. Apart from BVOC measurements, this database consists of carbon dioxide mixing ratios (LI-7500; LI-COR, Lincoln, Nebraska), meteorological conditions such as down-welling shortwave radiation (CNR4; Kipp & Zonen, Delft, Netherlands), temperature & relative humidity (HMP45; Vaisala, Helsinki, Finland), pressure (LI-7500; LI-COR, Lincoln, Nebraska), wind speed and wind direction (CSAT3; Campbell Scientific, Logan, Utah). The solar radiation measurements are made at a height of 41 m and the other measurements at a height of 35 m from the ground. Further, ecological information of the surrounding forest such as species composition and abundance is available at Chan et al. (2011).

2.2 Emissions model

Overview of approach. BVOC emissions are modeled using MEGAN (Model of Emissions of Gases and Aerosols from Nature), a widely recognized mechanistic model that estimates emissions of BVOCs in the atmosphere originating from terrestrial vegetation (Guenther et al., 2012). Leveraging inputs such as plant species, environmental conditions, and meteorological data, the model predicts BVOC emission rates, allowing us to understand their contributions to atmospheric processes. MEGANv3.2 is used in this work. Fundamentally, MEGAN estimates emissions flux (F_i) of chemical species i according to Equation (1)

$$F_i = \gamma_i \sum \epsilon_{i,j} \chi_j \quad (1)$$

where $\epsilon_{i,j}$ is the emission factor at standard conditions for vegetation type j . χ_j represents the fractional area of a model grid cell covered with vegetation. The emission activity factor (γ_i) accounts for the environmental and phenological conditions processes controlling emissions such as light (γ_P), temperature (γ_T), leaf age (γ_A), soil moisture (γ_{SM}), leaf area index (LAI) and CO₂ inhibition (γ_{CO_2}) as shown in Equation (2).

$$\gamma_i = C_{CELAI} \gamma_{P,i} \gamma_{T,i} \gamma_{A,i} \gamma_{SM,i} \gamma_{CO_2,i} \quad (2)$$

Emission activity factors describing light and temperature impacts are divided into light-dependent and -independent components as

$$\gamma_{P,i} = (1 - LDF_i) + LDF_i \gamma_{P_LDF} \quad \text{and} \quad \gamma_{T,i} = (1 - LDF_i) \gamma_{T_LIF,i} + LDF_i \gamma_{T_LDF,i} \quad (3)$$

In equation 3, LDF_i is the light-dependent fraction for compound i , γ_{P_LDF} is the light-dependent activity factor, which is based on measurements for isoprene (Guenther et al., 2006), and $\gamma_{T_LIF,i}$ and $\gamma_{T_LDF,i}$ are the light-independent and light-dependent fractions of the temperature activity factor for compound i as described by (Guenther et al., 2006).

Once BVOCs are emitted into the atmosphere, they undergo photochemical oxidation to produce secondary products. Therefore, to be able to compare our observations of BVOC concentrations with those modeled, we convert the BVOC emission rates estimated by MEGAN to concentrations using a 0-dimensional box-model. MEGANv3.2-derived BVOC emissions are provided as inputs to the Framework for 0-D Atmospheric Model (F0AM) box model to simulate photochemistry and estimate time resolved BVOC concentrations. The framework of this modeling process is shown in Figure 1.

MEGANv3.2 parameterization. MEGANv3.2 was run from January 2, 2020 to December 29, 2020. A lambert conformal projection of the United States was used as the grid area for the simulations, where emissions were modeled in the cells encompassing the VFRL site. Emission factors ($\epsilon_{i,j}$) for the VFRL site were calculated using the MEGAN Emission Factor Preprocessor (MEGAN3.21-EFP), available in Python (<https://bai.ess.uci.edu/megan/data-and-code/megan32>), using the tree species composition shown in Table S2 based on a previously reported vegetation survey (Chan et al., 2011); canopy type is 26.88% needleleaf (predominantly pine) and 73.12% broadleaf (predominantly oak). The standard conditions emission factor for each compound and compound class used in this study have been listed in Table S1. Leaf Area Index (LAI) was provided as an input from the Terra MODIS (Moderate Resolution Imaging Spectroradiometer) data product (Myneni et al., 2015), extracted as 8-day averages at the coordinates of the VFRL using the Application for Extracting and Exploring Analysis Ready Samples (AppEEARS, (AppEEARS Team, 2020)).

Essential meteorological data required by MEGANv3.2 includes temperature, pressure, wind speed, water vapor mixing ratio, and photosynthetically active radiation (PAR). Measurements of relative humidity (%) were converted to water vapor mixing ratio (kg/kg) based on temperature and pressure. Down-welling shortwave radiation (W/m²) measurements were multiplied by 0.5 to convert them to PAR (W/m²) based on previously reported estimates that half of all incoming radiation is

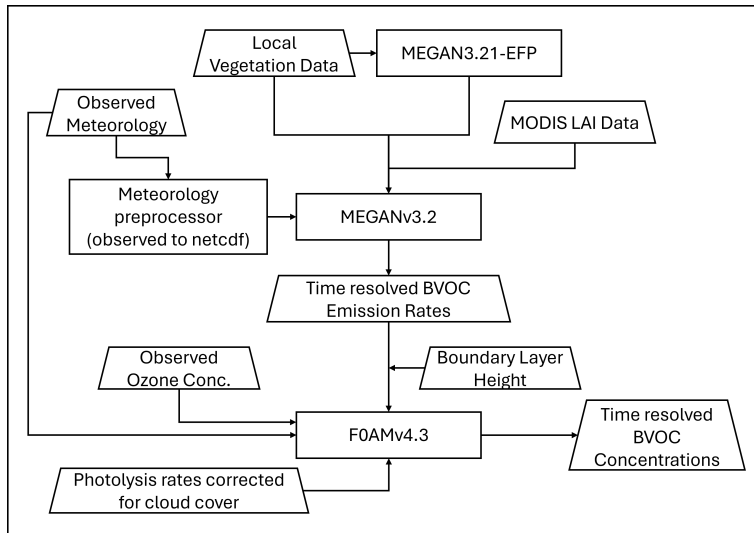


Figure 1. Modeling framework used to estimate time resolved local BVOC concentrations at the Virginia Forest Research Laboratory.

photosynthetically active (McCree, 1981). All meteorological measurements at VFRL were resampled to hourly data and converted to a gridded netcdf format suitable as input to MEGANv3.2. Gaps in observed meteorological data were filled with measurements from two personal weather stations (Weather Underground identifiers KVATROY19 and KVAPALMY31) located within 2 miles of VFRL as they are highly correlated with observed VFRL data (see Figure S3 for more information).

A soil type of silty-loam was used for the simulations (Soil Survey Staff, Natural Resources Conservation Service, United States Department of Agriculture, 2022). Soil temperature and soil moisture were obtained from the ERA5 (the fifth generation of the European Centre for Medium-Range Weather Forecasts Reanalysis) dataset (Hersbach et al., 2023) using the Open-Meteo API (Zippenfenig, 2023).

Simulations were run at different light dependent fractions (LDFs) to study the effect of changing emission profiles on diurnal variability of isoprene, α -pinene, limonene, and other monoterpenes. A summary of the model cases are listed in Table 1. The LDFs for α -pinene and limonene in MEGANv3.2 were changed to the results of positive matrix factorization (PMF) analysis conducted on the annual (September 2019 to September 2020) and summer (June, July, and August 2020) BVOC mixing ratios observed at VFRL (McGlynn et al., 2023a). The resulting timeseries of emission rates (in moles/s) for 200 compounds from MEGANv3.2 were converted to local emission fluxes (in nmol/m².s) by dividing emissions by the grid cell area.

2.3 F0AM setup

Photochemistry is modeled using the Framework for 0-D Atmospheric Model (F0AM v4.3 (Wolfe et al., 2016)) 0-dimensional box model that incorporates the Master Chemical Mechanism (MCM v3.3.1, (MCM)), with a starting point of the sample code 'ExampleSetup_DielCycle.m' available with that model. As the VFRL is located in a forest and the closest EPA measurements

Table 1. Summary of conditions tested in this study.

Label	Description	LDF _{α-pinene}	LDF _{limonene}
Default	LDFs used by default in MEGANv3.2	0.6	0.4
PMF _{Annual}	Fraction of concentrations attributed to light dependent factor from a PMF analysis of the annual VFRL dataset [†]	0.02	0.57
PMF _{Summer}	Fraction of concentrations attributed to light dependent factor from a PMF analysis of the VFRL summer dataset [†]	0.03	0.67
Case _{0.0-1.0}	Cases used for correlation studies 1 through 6	0, 0.2, 0.4, 0.6, 0.8, 1	0, 0.2, 0.4, 0.6, 0.8, 1
Adjusted	Time-dependent LDF based on correlation study	$f_1(t)$	$f_2(t)$

[†] McGlynn et al. (2023a); $f_1(t)$ & $f_2(t)$ as described in Figure 6

of NO_x mixing ratios are close to urban cities, NO₂ and NO values were constrained to those measured during the 2013 Southern Oxidant and Aerosol Study (SOAS, (Southern Oxidant and Aerosol Study, 2013)). Because direct measurements of NO_x at the tower were not available, ozone concentrations were constrained by observations rather than produced through photochemistry in the model. Hourly ozone mixing ratios were provided as those obtained from the nearest Environmental Protection Agency (EPA) AirData Air Quality monitors located at Albermale High School (roughly 15 miles Northwest of VFRL) using the Air Quality System (AQS) API v2 (US Environmental Protection Agency). Since ozone data at this site was only available between March and November of 2020, missing values in January through March were filled with those during 2021 from Shenandoah National Park (roughly 41 miles North of VFRL) and Prince Edward (roughly 53 miles South of VFRL). Missing values in November and December were filled with ozone mixing ratios measured at VFRL during 2019. Further, H₂ and CH₄ mixing ratios were constrained to 550 ppb and 1770 ppb respectively. Photolysis rates were calculated by the National Center for Atmospheric Research tropospheric ultraviolet and visible (TUV) transfer model (available at <https://www2.acom.ucar.edu/>) lookup tables as described by Wolfe et al. (2016). As this model estimates photolysis rates at clear cloud conditions, the rates were corrected using the method described by Equation 4 (Lu et al., 2017).

$$J_{corrected} = J_{TUV} \times \frac{SWR_{cloud}}{SWR_{clear}} \quad (4)$$

where $J_{corrected}$ is the corrected photolysis rate, J_{TUV} is the photolysis rate calculated from the TUV model lookup tables, SWR_{cloud} is the observed downwelling shortwave radiation at time t in W/m², and SWR_{clear} is the 7-day rolling maximum of the observed downwelling shortwave radiation in W/m² to represent clear-sky conditions. A constant 1st-order dilution rate of 1/day was used. Observed meteorological data for temperature, pressure, and relative humidity were used. OH concentrations were formed in-situ based on photolysis rates and observed concentrations of ozone and water vapor.

To incorporate the emission flux (in nmol/m².s) estimated by MEGANv3.2 into the F0AM chemical box model, 0th-order reactions were added to the chemical mechanism for each chemical compound, assuming instantaneous emission and mixing

160 into a box whose size was based on the boundary layer height (obtained from Dan Li (2020)). Observations in the AMDAR
dataset are available regularly but non-continuously throughout the year, and estimation of boundary layer height requires non-
trivial data analyses. Consequently, real-time estimates are not available and a 7-day rolling average of previously published
boundary layer heights for 2007 to 2019 are used (Dan Li, 2020). An average boundary layer height at airports IAD and RDU
are used. Though real-time boundary layer heights for 2020 are reported in the ERA5 dataset, prior work has shown these
estimates to be significantly different than observations, so are not used here (Zhang et al., 2020). The emission rate for F0AM
165 was hence calculated as in Equation 5,

$$k_{Emission,i} \left(\frac{\text{molecules}}{\text{cm}^3 \cdot \text{s}} \right) = F_i \left(\frac{\text{nmol}}{\text{m}^2 \cdot \text{s}} \right) \times 6.023 \times 10^{23} \left(\frac{\text{molecules}}{\text{mol}} \right) \times 10^{-9} \left(\frac{\text{mol}}{\text{nmol}} \right) \times \frac{1}{BLH(\text{m})} \times 10^{-6} \left(\frac{\text{m}^3}{\text{cm}^3} \right) \quad (5)$$

where F_i is the emission flux estimated by MEGANv3.2 for compound i , and BLH is the boundary layer height in m. These
settings were kept unchanged for all cases listed in Table 1. Results of the F0AM simulations allow us to compare simulated
and observed concentrations as reported in the following section.

170 **3 Results and Discussions**

3.1 Effect of changing LDF on emissions

175 Emissions peaks during the day, even with relatively high fractions of light-dependent emissions (Figure 2). Overall, light-
dependence has a stronger impact on night-time than on day-time concentrations. By decreasing the LDF of α -pinene (Figure
2c) from the default value of 0.6 to nearly 0 (0.02 and 0.03 in Annual and Summer cases respectively), nighttime emissions
increase by 139%-143%, and the daytime emissions increase by 47%-83%. Similarly, by increasing the LDF of limonene
(Figure 2b) from the default of 0.4 to 0.57 and 0.67 in the Annual and Summer cases respectively, we see a decrease in the
nighttime emissions ranging from 28%-45% and daytime emissions by 11%-29%. Since the LDF of isoprene was not changed
over any of the studies, the estimated emission diurnals remain unchanged (overlapping blue, red, and green lines in Figure 2),
but demonstrates the diurnal profile of a fully light-dependent compound (LDF of 1.0). These effects are observed across all
180 months, though the emission rates in the winter months are approximately 1-2% those in the summer months. Our observations
agree with Emmerson et al. (2018) who note that the nighttime monoterpene emissions in summer increase by 90%-100% when
LDF is turned off.

185 Given the impact of LDF on night-time emissions coupled with the typically low-boundary layer height at nighttime (which
will present as increased concentrations due to accumulation of emissions), it is important to more closely examine the LDFs
that best represent the observed concentrations of various compounds.

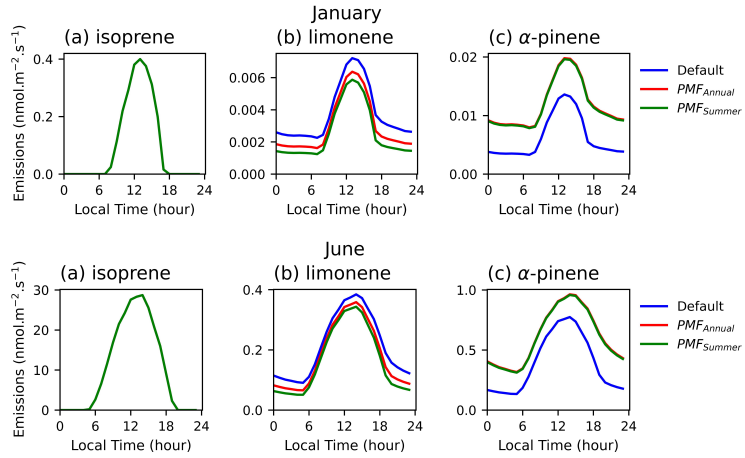


Figure 2. Monthly diurnal averages of the (a) isoprene, (b) limonene, and (c) α -pinene emissions (in $\text{nmol}/\text{m}^2\cdot\text{s}$) estimated by MEGANv3.2 at VFRL during January (top) and June (bottom) of 2020. The blue, red, and green lines indicate the Default ($\text{LDF}_{\text{isoprene}}=1$, $\text{LDF}_{\text{limonene}}=0.4$, $\text{LDF}_{\text{apinene}}=0.6$), $\text{PMF}_{\text{Annual}}$ ($\text{LDF}_{\text{isoprene}}=1$, $\text{LDF}_{\text{limonene}}=0.57$, $\text{LDF}_{\text{apinene}}=0.03$), and $\text{PMF}_{\text{Summer}}$ ($\text{LDF}_{\text{isoprene}}=1$, $\text{LDF}_{\text{limonene}}=0.67$, $\text{LDF}_{\text{apinene}}=0.02$) conditions as described in Table 1.

3.2 Measured vs. modeled BVOC concentrations

Modeled concentrations of monoterpenes generally have maxima in the evening, which agrees with α -pinene observations but is in contrast to summertime limonene (Figure 3). For all monoterpenes, even though observed wintertime concentrations are lower than those in the summer, the model still substantially underestimates concentrations in winter and spring (January to

190 May). Prior studies comparing observed concentrations with those simulated were carried out in peak summer and hence find relatively good agreement (Sindelarova et al., 2014). Concentrations of isoprene were below levels of detection of the GC-FID system through the winter, in contrast to low, but non-zero, emissions modeled for isoprene. Modeled and observed concentrations in the summer months are comparable in magnitude for all three compounds in the summer, and some day-to-day variability is also captured (4). Some day-to-day deviations between modeled and measured concentrations are expected, as 195 boundary layer heights and some atmospheric composition data are averages, which cannot capture real-world variability. Although there are no isoprene emissions during night-time (Figure 3), non-zero night-time isoprene concentrations are observed, which may suggest that nighttime chemistry and/or dilution may not be fully captured (Figure 4).

As noted in (McGlynn et al., 2023a), limonene in summer follow daytime peaks in concentration consistent with partially light-dependent behavior, and night-time peaks during winter. The model fails to capture these observed trends, either with 200 default LDF values or with those estimated using the fraction of limonene estimated as light-dependent based on factorization ($\sim 60\%$). In contrast, α -pinene has nighttime peaks, which are approximately captured by default values and by changing the LDF to 0.03. Importantly, it is clear that the LDF that best captures observed variability may vary throughout the year, indicating important seasonality.

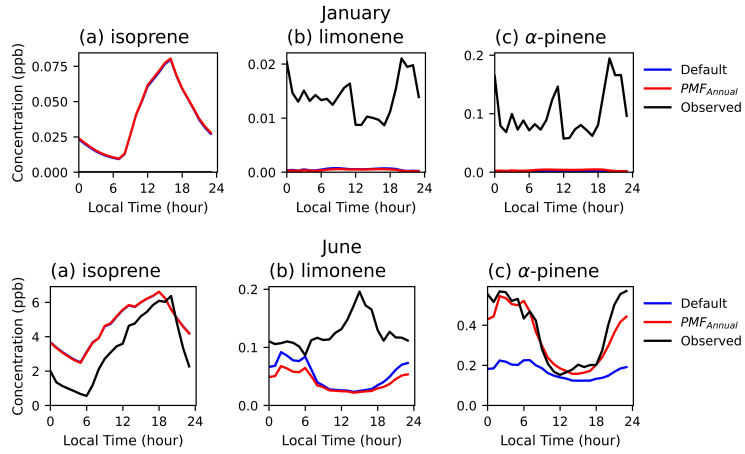


Figure 3. Monthly diurnal averages of the (a) isoprene, (b) limonene, and (c) α -pinene concentrations (in ppb) estimated by MEGANv3.2 and F0AM at VFRL during January (top) and June (bottom) of 2020. The blue and red lines indicate the Default ($LDF_{isoprene}=1$, $LDF_{limonene}=0.4$, $LDF_{\alpha\text{-pinene}}=0.6$) and PMF_{Annual} ($LDF_{isoprene}=1$, $LDF_{limonene}=0.57$, $LDF_{\alpha\text{-pinene}}=0.03$) conditions as described in Table 1, and black lines indicate observed data. Observed concentrations for isoprene were below GC-FID limits of detection for January 2020.

3.3 Monthly variation of LDF

205 To understand the variation of LDF throughout the year, we ran MEGAN simulations at 6 different values of $LDF_{\alpha\text{-pinene}}$ and $LDF_{limonene}$: 0, 0.2, 0.4, 0.6, 0.8, and 1. Emissions from each scenario were provided to the F0AM model and a snapshot of the results from July 2020 are as shown in Figure 5 compared to observed data. As expected from previous studies, concentrations of α -pinene correlate well with low values of LDF (5b). While low LDF values for limonene better match observations in absolute magnitude, they substantially invert the observed diurnality. Instead, observed concentrations of limonene correlate 210 best with high values of LDF (cyan line in Figure 5a) though absolute concentrations are underpredicted. To better quantify the monthly variation of LDF with the highest correlation with observed concentrations, linear interpolation between emissions scenarios was used to estimate emissions at resolution of 0.01 LDF. The light dependency that best correlates with observations varies throughout the year (Figure 6), with a peak in light dependence during the summer and less light-dependence during the rest of the year. Conversely, a constant $LDF_{\alpha\text{-pinene}}$ of 0 (i.e., light-independent) throughout the year slightly improves the 215 correlation coefficient.

Simulations were re-run using the LDF value for each month that maximizes correlation (Figure 7, for α -pinene see Figure S4). In the month of January, there is no discernible increase in correlation by changing the LDF and the modeled concentrations are extremely low. In the summer (Figure 7a), the correlation between the simulations and the observed concentrations improves from -0.01 to 0.49 by changing the LDF from a default value of 0.4 to a value of 0.97. However, the magnitude 220 of the modeled concentrations remains low, suggesting underpredicted emission rates. In September (Figure 7b), there is no

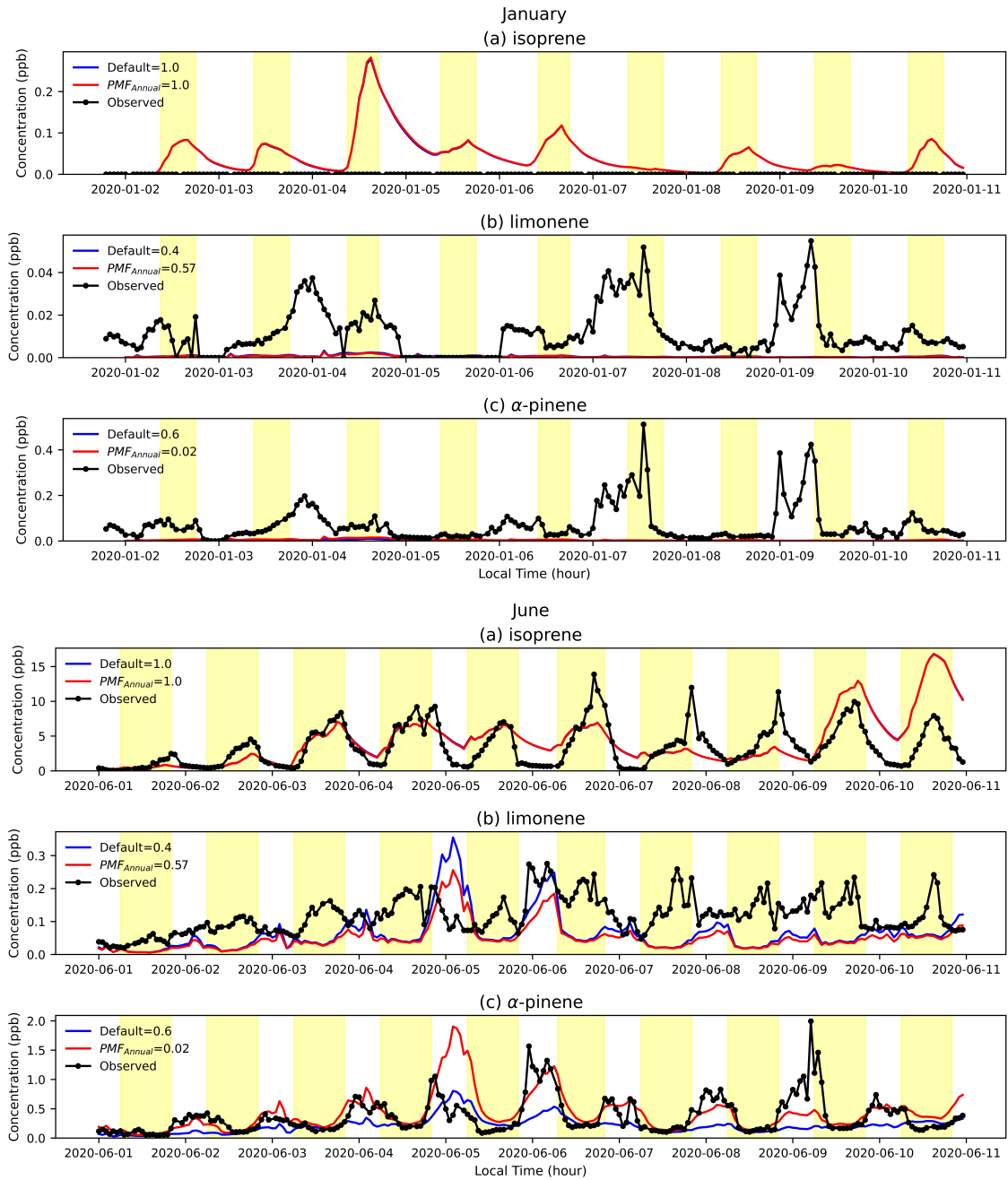


Figure 4. A snapshot of concentrations (in ppb) of (a) isoprene, (b) limonene, and (c) α -pinene estimated by MEGANv3.2 and F0AM at VFRL during January (top) and June (bottom) of 2020. The blue and red lines indicate the Default and PMF_{Annual} conditions as described in Table 1, and black lines indicate observed data. Observed concentrations for isoprene were below GC-FID limits of detection for January 2020.

significant change in the correlation by changing LDF as the diurnal shapes are similar below an LDF of 0.8 but the magnitude of the concentrations at the adjusted LDFs are closer to those observed.

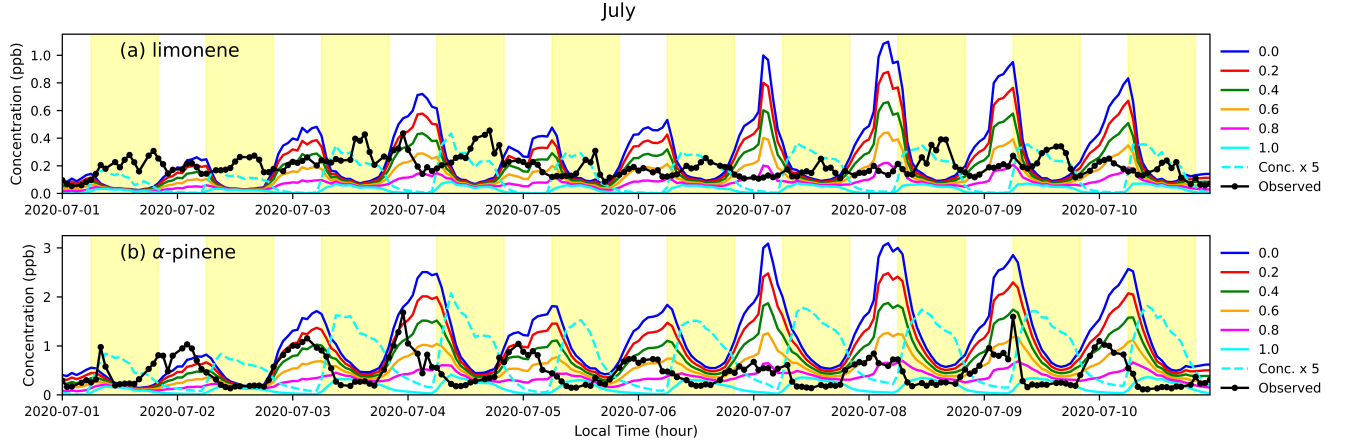


Figure 5. A snapshot of (a) limonene and (b) α -pinene concentrations (in ppb) estimated by MEGANv3.2 and F0AM at VFRL during July of 2020. The blue, red, green, orange, magenta, cyan lines refer to simulations with LDF set to 0, 0.2, 0.4, 0.6, 0.8, and 1 respectively (Table 1), and black lines indicate observed data. The dashed cyan line represents the simulated concentrations for LDF=1.0 multiplied by 5. Daytime hours are highlighted in yellow.

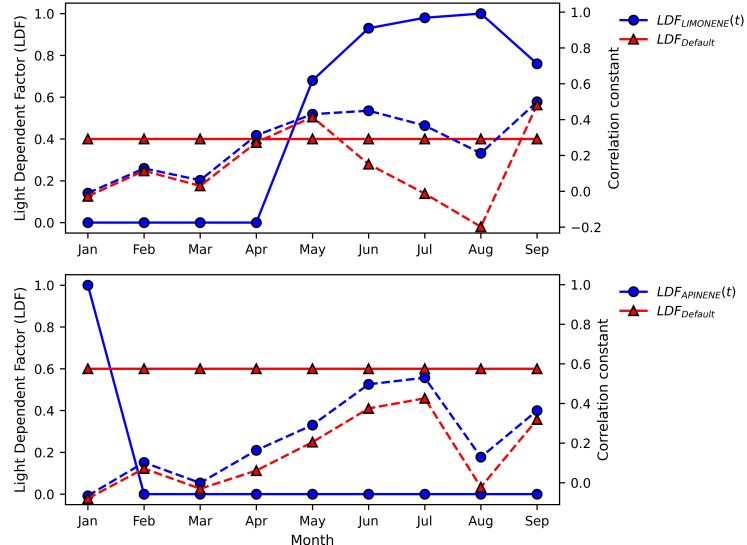


Figure 6. Monthly variation of LDF for limonene and α -pinene estimated by maximizing the correlation between observed concentrations and those estimated by MEGANv3.2 and F0AM at VFRL. The blue circles and red triangles marked solid lines represent the time-dependent and Default LDF values respectively and the dashed lines represent the corresponding Pearson correlation coefficients.

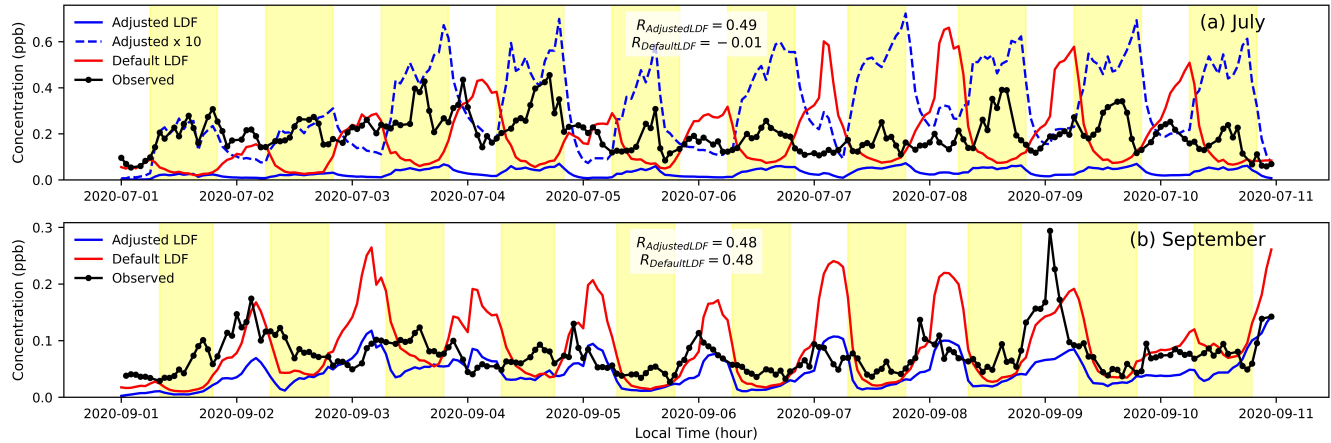


Figure 7. A snapshot of limonene concentrations (in ppb) for July, and September of 2020 using the monthly LDF as shown in Figure 6. The dashed blue line represents the simulated concentrations for Adjusted LDF multiplied by 10. The Pearson correlation coefficient values of the adjusted and default modeled (refer to Table 1) concentrations against the observed concentrations are reported as $R_{\text{AdjustedLDF}}$ and $R_{\text{DefaultLDF}}$.

3.4 Extension of F0AM for other BVOCs

Currently, MCM3.3.1 used during F0AM simulations contains only isoprene and 3 monoterpenes: isoprene, α -pinene, β -pinene, and limonene. To simulate the concentrations of other compounds measured at VFRL, we added dummy chemical reactions in the MCM to simulate the chemical loss of other BVOCs emitted into the box for which observational data are available. The reaction rates used are as listed in Table S5.

Following the method described in Section 3.3, the monthly variation of sabinene is as shown in Figure 8 and those of α -fenchene, β -phellandrene, β -thujene, camphene, tricyclene and γ -terpinene in Figure S6. Sabinene is observed to be almost completely light dependent in the summer, with strong daytime peaks (Figures 8 and 9). Similarly, variation of LDFs for β -thujene and γ -terpinene follows a similar pattern to that of limonene where the LDF peaks in the summer and falls off during the rest of the year. β -phellandrene shows no significant increase in correlation for LDFs between 0-0.8 but the correlation deteriorates to negative values (Figure S7) if we assume it is completely light-dependent (LDF=1). By default, MEGANv3.2 assigns the limonene compound class LDF for β -phellandrene and γ -terpinene (LDF=0.4), and carene compound class LDF for sabinine, α -fenchene, β -thujene, camphene, and tricyclene (LDF=0.2). It is interesting to note that MEGANv3.2 assumes that sabinene, β -thujene, and γ -terpinene are partially light-dependent throughout the year, despite more appropriate summertime LDFs of around 1. The results in this study corroborate the PMF observations by McGlynn et al. (2023a) which note that β -thujene, sabinine, γ -terpinene, and β -phellandrene display light-dependent behaviors. Further, α -fenchene and camphene behave similar to α -pinene where they remain completely light-independent throughout the year (as opposed to the 0.2 LDF assumed in the MEGAN model).

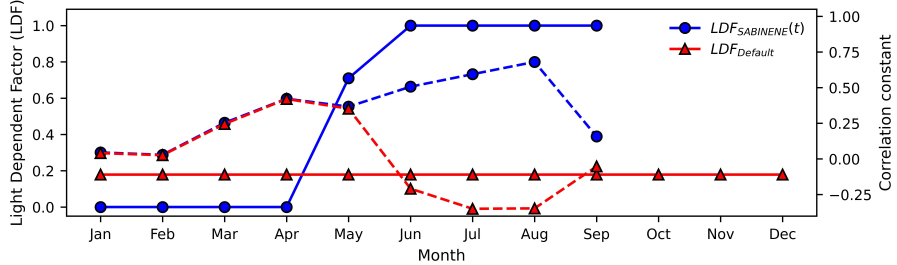


Figure 8. Monthly variation of LDF for sabinene estimated by maximizing the correlation between observed concentrations and those estimated by MEGANv3.2 and F0AM at VFRL. The blue circles represent the adjusted LDF values, the red triangles represents the LDF used by default in MEGANv3.2. The blue and red dashed lines present the LDF values and the dashed lines represent the corresponding Pearson correlation coefficients.

Simulations were run at an LDF of 1 (highest correlation, Figure 8) for sabinine in July and September. Upon correcting the LDF to be completely light-dependent, sabinine concentrations peak during the daytime to match the diurnals of observed concentrations. Similar to limonene, the magnitudes remain underpredicted. Overall, the variability of LDF throughout the year and the deviation from the values currently used suggests that there is an important seasonality to LDF that needs to be incorporated into emissions models.

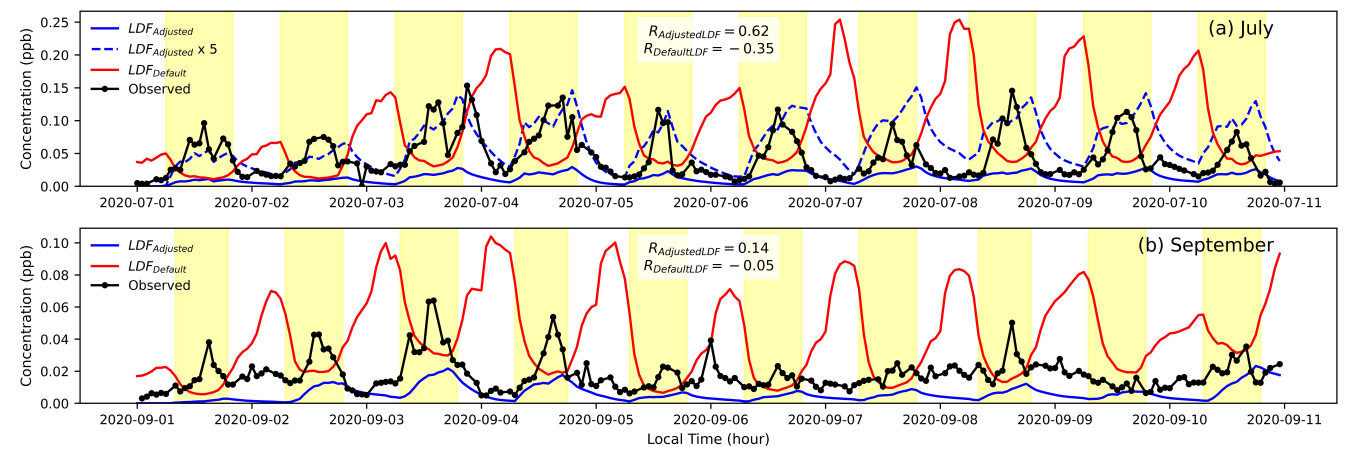


Figure 9. A snapshot of sabinene concentrations (in ppb) for July, and September of 2020 using the monthly LDF as shown in Figure 8. The dashed blue line represents the simulated concentrations for adjusted LDF multiplied by 5.

4 Conclusions

In this study, we used MEGANv3.2 to simulate BVOC emissions during the year 2020 at a southeastern U.S. forest using local ecological and meteorological data. The photochemistry was simulated by F0AM v4.3 to obtain speciated concentration

timeseries. Prior work at this site shows that the LDFs used in these models contradict the light dependent contribution of
250 some monoterpenes estimated from observed diurnals (McGlynn et al., 2023a). In this work, we demonstrate that LDFs for monoterpenes used by default in the models are not consistent with the observed diurnal and seasonal patterns. We observe an LDF _{α -pinene} value of 0 (as opposed to 0.6) and a time-dependent LDF_{limonene} of 0 for January through April and roughly 0.74-0.97 in the summer months as described in Figure 6. Further, we were able to extend the model to simulate concentrations of other monoterpenes to get speciated information at our local site. We note that LDFs of α -pinene-like bicyclic monoterpenes
255 camphene and α -fenchene follow light-independent behavior throughout the year much like the α -pinene. Further, molecules with structures similar to limonene-like such as β -thujene, and bicyclic monoterpenes with a 5-carbon ring such as sabinene, and γ -terpinene have an LDF that varies throughout the year (like limonene), with light-dependent behavior in summer and light-independent behavior in winter and spring. Lastly, we note that the simulations fail to capture observed concentrations in the winter months where they are consistently underpredicted. In contrast, we are able to capture the day-to-day variability
260 in the concentrations during summer months using this relatively simple setup of MEGAN and a 0-D box model with 7-day rolling average of the boundary layer height conditions, and NO_x and O₃ concentrations from non-local sources.

This study underscores the need for significant improvements in the LDF within BVOC emission models, particularly for monoterpenes, to more accurately reflect the complex nature of BVOC emissions under varying lighting conditions. The observed seasonality in LDF for specific monoterpenes highlights the importance of incorporating temporal changes into
265 these models. The implications of this research are wide-ranging. Enhancing the precision of BVOC emission models can lead to more accurate forecasts of atmospheric chemistry, which in turn impacts air quality and climate. Improved models will also aid in better understanding the role of BVOCs in the formation of ozone and secondary organic aerosols (SOAs), both of which have significant environmental and health impacts. Additionally, acknowledging the seasonality in LDF can guide the development of dynamic models that adjust for seasonal variations in monoterpene emissions, thereby increasing the accuracy
270 of emission inventories, especially in regions with pronounced seasonal shifts. Further, the LDF seasonality has important implications on the biology underlying terpene production and emission. Earlier studies have suggested a positive relationship between light dependency and lack of storage of terpene compounds e.g., Lerdau and Gray (2003), and the results presented here suggest that metabolic pathways and storage processes may vary both among and within compounds over the course of the year. Compounds showing higher LDFs may be serving as responses to factors that vary with light intensity, so storage is
275 less beneficial, while those with low LDFs are more analogous to constitutive compounds that function in response to factors that act independently of light. Similar results have been shown for certain floral volatiles (Theis et al., 2007), but this study is the first to report such findings for leaf volatiles. Overall, our findings highlight the urgent need for continuous refinement of BVOC emission models. By incorporating more precise LDF parameters and considering seasonal dynamics, we can deepen our comprehension of the interactions between the biosphere and atmosphere, and their broader effects on climate and public
280 health.

Code and data availability. Data required to run simulations are provided in Tables plotted in the main results are provided in Tables S1, S2, and S5. Raw data (i.e., meteorological and BVOC concentrations) are available by request by contacting the corresponding author.

Author contributions. NSP: conceptualization, data curation, methodology, investigation, writing (original draft), formal analysis, visualization. GI-VW: conceptualization, methodology, writing (review and editing), supervision, funding acquisition. DFM: conceptualization, data curation, writing (review and editing). LEB: writing (review and editing), data curation. TMD: data curation, writing (review and editing). MTL: conceptualization, writing (review and editing). SEP: conceptualization, writing (review and editing), supervision, funding acquisition.

Competing interests. The authors declare that they have no conflict of interest.

Acknowledgements. This research was funded by the National Science Foundation (AGS 1837882, AGS 1837891, and AGS 2046367).

References

290 AppEEARS Team: Application for extracting and exploring analysis ready samples (AppEEARS), Sioux Falls, South Dakota, USA: NASA EOSDIS Land Processes Distributed Active Archive Center (LP DAAC), USGS/Earth Resources Observation and Science (EROS) Center, 2020.

Atkinson, R.: Atmospheric chemistry of VOCs and NO_x, *Atmospheric environment*, 34, 2063–2101, 2000.

Atkinson, R. and Arey, J.: Gas-phase tropospheric chemistry of biogenic volatile organic compounds: a review, *Atmospheric Environment*, 295 37, 197–219, 2003.

Calfapietra, C., Pallozzi, E., Lusini, I., and Velikova, V.: Modification of BVOC emissions by changes in atmospheric [CO₂] and air pollution, *Biology, controls and models of tree volatile organic compound emissions*, pp. 253–284, 2013.

Chan, W.-Y. S., Fuentes, J., Lerdau, M., Shugart, H., Scanlon, T., and Clarens, A.: The Fate of Biogenic Hydrocarbons within a Forest Canopy: Field Observation and Model Results, Ph.D. thesis, University of Virginia, 2011.

300 Chen, J., Tang, J., and Yu, X.: Environmental and physiological controls on diurnal and seasonal patterns of biogenic volatile organic compound emissions from five dominant woody species under field conditions, *Environmental Pollution*, 259, 113 955, 2020.

Dan Li: AMDAR-BL-PBLH-DATASET, Available online, <https://zenodo.org/record/3934378>, 2020.

Debevec, C. and Sauvage, S.: Temporal and spatial variabilities of volatile organic compounds in the Mediterranean atmosphere, in: *Atmospheric Chemistry in the Mediterranean Region: Volume 1-Background Information and Pollutant Distribution*, pp. 505–536, Springer, 305 2023.

Dindorf, T., Kuhn, U., Ganzeveld, L., Schebeske, G., Ciccioli, P., Holzke, C., Köble, R., Seufert, G., and Kesselmeier, J.: Significant light and temperature dependent monoterpene emissions from European beech (*Fagus sylvatica* L.) and their potential impact on the European volatile organic compound budget, *Journal of Geophysical Research: Atmospheres*, 111, 2006.

Ebi, K. L. and McGregor, G.: Climate change, tropospheric ozone and particulate matter, and health impacts, *Environmental Health Perspectives*, 310 116, 1449–1455, 2008.

Emmerson, K. M., Cope, M. E., Galbally, I. E., Lee, S., and Nelson, P. F.: Isoprene and monoterpene emissions in south-east Australia: comparison of a multi-layer canopy model with MEGAN and with atmospheric observations, *Atmospheric Chemistry and Physics*, 18, 7539–7556, 2018.

Fiscus, E. L., Booker, F. L., and Burkey, K. O.: Crop responses to ozone: uptake, modes of action, carbon assimilation and partitioning, *Plant, Cell & Environment*, 28, 997–1011, 2005.

315 Goldstein, A. H. and Galbally, I. E.: Known and unexplored organic constituents in the earth's atmosphere, *Environmental Science Technology*, 41, 1514–1521, 2007.

Guenther, A., Hewitt, C. N., Erickson, D., Fall, R., Geron, C., Graedel, T., Harley, P., Klinger, L., Lerdau, M., McKay, W., et al.: A global model of natural volatile organic compound emissions, *Journal of Geophysical Research: Atmospheres*, 100, 8873–8892, 1995.

320 Guenther, A., Karl, T., Harley, P., Wiedinmyer, C., Palmer, P. I., and Geron, C.: Estimates of global terrestrial isoprene emissions using MEGAN (Model of Emissions of Gases and Aerosols from Nature), *Atmospheric Chemistry and Physics*, 6, 3181–3210, 2006.

Guenther, A., Jiang, X., Heald, C. L., Sakulyanontvittaya, T., Duhl, T. a., Emmons, L., and Wang, X.: The Model of Emissions of Gases and Aerosols from Nature version 2.1 (MEGAN2. 1): an extended and updated framework for modeling biogenic emissions, *Geoscientific Model Development*, 5, 1471–1492, 2012.

325 Helmig, D., Ortega, J., Duhl, T., Tanner, D., Guenther, A., Harley, P., Wiedinmyer, C., Milford, J., and Sakulyanontvittaya, T.: Sesquiterpene emissions from pine trees- identifications, emission rates and flux estimates for the contiguous United States, *Environmental science & technology*, 41, 1545–1553, 2007.

Herbinger, K., Then, C., Haberer, K., Alexou, M., Löw, M., Remele, K., Rennenberg, H., Matyssek, R., Grill, D., Wieser, G., et al.: Gas exchange and antioxidative compounds in young beech trees under free-air ozone exposure and comparisons to adult trees, *Plant Biology*, 330 9, 288–297, 2007.

Hersbach, H., Bell, B., Berrisford, P., Biavati, G., Horányi, A., Muñoz Sabater, J., Nicolas, J., Peubey, C., Radu, R., Rozum, I., et al.: ERA5 hourly data on single levels from 1940 to present, *Copernicus Climate Change Service (C3S) Climate Data Store (CDS)*, 2023.

Holopainen, J. K.: Multiple functions of inducible plant volatiles, *Trends in plant science*, 9, 529–533, 2004.

Holopainen, J. K. and Gershenson, J.: Multiple stress factors and the emission of plant VOCs, *Trends in plant science*, 15, 176–184, 2010.

335 Huang, J., Hartmann, H., Hellén, H., Wisthaler, A., Perreca, E., Weinhold, A., Rućker, A., van Dam, N. M., Gershenson, J., Trumbore, S., et al.: New perspectives on CO₂, temperature, and light effects on BVOC emissions using online measurements by PTR-MS and cavity ring-down spectroscopy, *Environmental science & technology*, 52, 13 811–13 823, 2018.

Kampa, M. and Castanas, E.: Human health effects of air pollution, *Environmental pollution*, 151, 362–367, 2008.

Kivimäenpää, M., Ghimire, R. P., Sutinen, S., Häikiö, E., Kasurinen, A., Holopainen, T., and Holopainen, J. K.: Increases in volatile organic 340 compound emissions of Scots pine in response to elevated ozone and warming are modified by herbivory and soil nitrogen availability, *European journal of forest research*, 135, 343–360, 2016.

Lerdau, M. and Gray, D.: Ecology and evolution of light-dependent and light-independent phytogenic volatile organic carbon, *New Phytologist*, 157, 199–211, 2003.

Li, Z. and Sharkey, T. D.: Metabolic profiling of the methylerythritol phosphate pathway reveals the source of post-illumination isoprene 345 burst from leaves, *Plant, Cell & Environment*, 36, 429–437, 2013.

Lindwall, F., Faubert, P., and Rinnan, R.: Diel variation of biogenic volatile organic compound emissions-a field study in the sub, low and high arctic on the effect of temperature and light, *PloS one*, 10, e0123 610, 2015.

Liu, Y., Li, L., An, J., Huang, L., Yan, R., Huang, C., Wang, H., Wang, Q., Wang, M., and Zhang, W.: Estimation of biogenic VOC emissions and its impact on ozone formation over the Yangtze River Delta region, China, *Atmospheric Environment*, 186, 113–128, 2018.

350 Llusia, J., Penuelas, J., Alessio, G. A., and Estiarte, M.: Contrasting species-specific, compound-specific, seasonal, and interannual responses of foliar isoprenoid emissions to experimental drought in a Mediterranean shrubland, *International Journal of Plant Sciences*, 169, 637–645, 2008.

Lu, X., Chen, N., Wang, Y., Cao, W., Zhu, B., Yao, T., Fung, J. C., and Lau, A. K.: Radical budget and ozone chemistry during autumn in the atmosphere of an urban site in central China, *Journal of Geophysical Research: Atmospheres*, 122, 3672–3685, 355 <https://doi.org/10.1002/2016JD025676>, 2017.

Lu, X., Zhang, L., and Shen, L.: Meteorology and climate influences on tropospheric ozone: a review of natural sources, chemistry, and transport patterns, *Current Pollution Reports*, 5, 238–260, 2019.

McCree, K. J.: Photosynthetically active radiation, in: *Physiological plant ecology I: Responses to the physical environment*, pp. 41–55, Springer, 1981.

360 McGlynn, D. F., Barry, L. E., Lerdau, M. T., Pusede, S. E., and Isaacman-VanWertz, G.: Measurement report: Variability in the composition of biogenic volatile organic compounds in a Southeastern US forest and their role in atmospheric reactivity, *Atmospheric Chemistry and Physics*, 21, 15 755–15 770, 2021.

McGlynn, D. F., Frazier, G., Barry, L. E., Lerdau, M. T., Pusede, S. E., and Isaacman-VanWertz, G.: Minor contributions of daytime monoterpenes are major contributors to atmospheric reactivity, *Biogeosciences*, 20, 45–55, 2023a.

365 McGlynn, D. F., Panji, N. S., Frazier, G., Bi, C., and Isaacman-VanWertz, G.: An autonomous remotely operated gas chromatograph for chemically resolved monitoring of atmospheric volatile organic compounds, *Environmental Science: Atmospheres*, 3, 387–398, 2023b.

McGlynn, Deborah; Isaacman-VanWertz, G.: In-Canopy Biogenic Volatile Organic Compounds Mixing Ratios at the Virginia Forest Lab, Available online, <https://doi.org/https://websoilsurvey.nrcs.usda.gov/app/>, 2022.

MCM: Master Chemical Mechanism v3.3.1, <https://mcm.york.ac.uk/>.

370 Myhre, G., Shindell, D., Bréon, F., Collins, W., Fuglestvedt, J., Huang, J., Koch, D., Lamarque, J., Lee, D., Mendoza, B., Nakajima, T., Robock, A., Stephens, G., Takemura, T., and Zhang, H.: Anthropogenic and natural radiative forcing, *Climate Change 2013-The Physical Science Basis. Contribution of Working Group I to the Fifth Assessment Report of the Intergovernmental Panel on Climate Change*, 2014.

Myneni, R., Knyazikhin, Y., and Park, T.: MOD15A2H MODIS/Terra leaf area Index/FPAR 8-Day L4 global 500m SIN grid V006, NASA EOSDIS Land Processes DAAC, <https://doi.org/10.5067/MODIS/MOD15A2H.006>, 2015.

375 Pollmann, J., Ortega, J., and Helmig, D.: Analysis of atmospheric sesquiterpenes: Sampling losses and mitigation of ozone interferences, *Environmental science & technology*, 39, 9620–9629, 2005.

Rasmussen, R. A. and Went, F.: Volatile organic material of plant origin in the atmosphere, *Proceedings of the National Academy of Sciences*, 53, 215–220, 1965.

Sadiq, M., Tai, A. P., Lombardozzi, D., and Val Martin, M.: Effects of ozone–vegetation coupling on surface ozone air quality via biogeо-380 chemical and meteorological feedbacks, *Atmospheric Chemistry and Physics*, 17, 3055–3066, 2017.

Safieddine, S. A., Heald, C. L., and Henderson, B. H.: The global nonmethane reactive organic carbon budget: A modeling perspective, *Geophysical Research Letters*, 44, 3897–3906, 2017.

Sanadze, G.: Light-dependent excretion of molecular isoprene, *Prog Photosynth Res*, 2, 701–707, 1969.

Sindelarova, K., Granier, C., Bouarar, I., Guenther, A., Tilmes, S., Stavrakou, T., Müller, J.-F., Kuhn, U., Stefani, P., and Knorr, W.: Global 385 data set of biogenic VOC emissions calculated by the MEGAN model over the last 30 years, *Atmospheric Chemistry and Physics*, 14, 9317–9341, 2014.

Situ, S., Guenther, A., Wang, X., Jiang, X., Turnipseed, A., Wu, Z., and Bai, J.: Impacts of seasonal and regional variability in biogenic VOC emissions on surface ozone in the Pearl River delta region, China, *Atmospheric Chemistry and Physics*, 13, 11 803–11 817, 2013.

Soil Survey Staff, Natural Resources Conservation Service, United States Department of Agriculture: Web Soil Survey, Available online, 390 <https://websoilsurvey.nrcs.usda.gov/app/>, accessed: January 25, 2024, 2022.

Southern Oxidant and Aerosol Study: Southern Oxidant and Aerosol Study, Available online, https://www.eol.ucar.edu/field_projects/sas, 2013.

Theis, N., Lerdau, M., and Raguso, R. A.: The challenge of attracting pollinators while evading floral herbivores: patterns of fragrance emission in *Cirsium arvense* and *Cirsium repandum* (Asteraceae), *International Journal of Plant Sciences*, 168, 587–601, 2007.

395 US Environmental Protection Agency: Air Quality System Data Mart, Available online, <https://www.epa.gov/outdoor-air-quality-data>, accessed: February 16, 2024.

Wolfe, G. M., Marvin, M. R., Roberts, S. J., Travis, K. R., and Liao, J.: The framework for 0-D atmospheric modeling (F0AM) v3. 1, *Geoscientific Model Development*, 9, 3309–3319, 2016.

Yang, Q., Gustafson Jr, W., Fast, J. D., Wang, H., Easter, R. C., Morrison, H., Lee, Y.-N., Chapman, E. G., Spak, S., and Mena-Carrasco, M.:
400 Assessing regional scale predictions of aerosols, marine stratocumulus, and their interactions during VOCALS-REx using WRF-Chem, Atmospheric Chemistry and Physics, 11, 11 951–11 975, 2011.

Yu, H. and Blande, J. D.: Diurnal variation in BVOC emission and CO₂ gas exchange from above-and belowground parts of two coniferous species and their responses to elevated O₃, Environmental Pollution, 278, 116 830, 2021.

Zhang, M., Zhao, C., Yang, Y., Du, Q., Shen, Y., Lin, S., Gu, D., Su, W., and Liu, C.: Modeling sensitivities of BVOCs to different versions of
405 MEGAN emission schemes in WRF-Chem (v3. 6) and its impacts over eastern China, Geoscientific Model Development, 14, 6155–6175, 2021.

Zhang, Y., Sun, K., Gao, Z., Pan, Z., Shook, M. A., and Li, D.: Diurnal climatology of planetary boundary layer height over the contiguous United States derived from AMDAR and reanalysis data, Journal of Geophysical Research: Atmospheres, 125, e2020JD032 803, 2020.

Zheng, Y., Unger, N., Barkley, M. P., and Yue, X.: Relationships between photosynthesis and formaldehyde as a probe of isoprene emission,
410 Atmospheric Chemistry and Physics, 15, 8559–8576, 2015.

Zippenfenig, P.: Open-Meteo.com Weather API, <https://doi.org/10.5281/zenodo.7970649>, 2023.